Influence of Ta content on the physical properties of $SrBi_2Ta_2O_9$ ferroelectric thin films

Fan-Yi Hsu
Department of Materials Science and Engineering, National Tsing Hua University, Hsinchu 30013, Taiwan, Republic of China

Ching-Chich Leu
Department of Chemical and Materials Engineering, National University of Kaohsiung, Kaohsiung 811, Taiwan, Republic of China

Chao-Hsin Chien
Department of Electronics Engineering, National Chiao Tung University, Hsinchu 30050, Taiwan, Republic of China

Chen-Ti Hu[a]
Department of Materials Science and Engineering, National Tsing Hua University, Hsinchu 30013, Taiwan, Republic of China

(Received 17 March 2006; accepted 16 August 2006)

We have investigated the effect that the Ta content has on the ferroelectric properties of strontium bismuth tantalate (SBT) thin films synthesized using metalorganic decomposition (MOD) and spin coating techniques. The physical properties of these SBT samples were strongly dependent upon the Ta ratio. Polarization measurements revealed that Ta-deficient SBT exhibited a relatively low coercive field ($2E_c$ ~ 87 kV/cm) and a high remanent polarization ($2P_r$ ~ 15 μC/cm^2). The value of $2P_r$ decreased as the Ta ratio in SBT increased. The improved ferroelectric properties of the Ta-deficient SBT samples may have resulted from the uniformly well-grown bismuth-layered-structured (BLS) phases of the films and their highly preferential orientation along the *a* and *b* axes. We suggest that the incorporation of Ta vacancies plays an important role in enhancing the crystallinities and microstructures of Ta-deficient SBT films.

I. INTRODUCTION

Although strontium bismuth tantalate ($SrBi_2Ta_2O_9$, SBT) is one of the most promising materials for application in nonvolatile random access memories (it displays several excellent ferroelectric properties, such as a low leakage current, low operating voltage, and fatigue endurance for up to 10^{12} switching cycles),[1] its high crystallization temperature (>750 °C), which is obviously incompatible with conventional very large scale integrated (VLSI) processes, and the relatively low remanent polarization of SBT thin films remain major obstacles for its deployment.

Ferroelectric SBT thin films have been grown using many techniques, including metalorganic decomposition (MOD),[2] pulsed laser deposition (PLD),[3] and metalorganic chemical vapor deposition (MOCVD).[4] The MOD method in particular offers a number of advantages, such as good homogeneity, long shelf-life, precise control over the composition, low cost, and simplicity.[5] It is well known that the ferroelectric properties of SBT thin films along the *a* and *b* axes are much better than those along the *c* axis.[6] Thus, the texture of SBT thin film is an important factor for determining its electrical properties. MOD is not, however, an effective method when attempting to control the crystalline orientation. A number of techniques are used to manipulate the film orientation during wet chemical depositions such as the MOD and sol-gel methods, for example, utilizing the appropriate substrates with either a matching lattice or suitable buffer layers.[7,8] Alternatively, modifications of the precursor solutions, film compositions, and heat treatment process may also be used to affect the film's crystallinity and texture.[9,10] SBT thin films containing Sr and Bi contents deviating from stoichiometry have been studied for many years.[11] The crystalline structures and ferroelectric properties are influenced markedly through small compositional changes. In Bi-excess and Sr-deficient SBT samples, Sr sites are inhabited by Bi ions.[12,13] Shimakawa et al. reported that the substitution of small Bi^{3+}

[a]Address all correspondence to this author.
e-mail: cthu@mx.nthu.edu.tw
DOI: 10.1557/JMR.2006.0383

 © 2006 Materials Research Society
CAMBRIDGE JOURNALS http://journals.cambridge.org Downloaded: 26 Apr 2014 IP address: 140.113.38.11

ions for large Sr^{2+} ions causes pronounced compressive stress in the perovskite-like unit. This mismatch between the perovskite-like unit and the Bi_2O_2 interlayer leads to great distortion of the TaO_6 octahedra, resulting, consequently, in a SBT sample displaying a large spontaneous polarization and a high Curie temperature.[14] Chen et al. have attributed the enhancement in P_r to the large average grain sizes of Sr-deficient SBT.[15] The value of P_r decreases, however, when the Sr ratio becomes too low, presumably because of the formation of Sr vacancies and the appearance of a second phase ($BiTaO_4$).[15,16]

Recently, we reported that the film properties of SBT are improved when using an ultrathin Ta (<1 nm) buffer layer.[17] The Ta buffer layer causes the SBT composition to depart from stoichiometry to form a Ta-enriched region near the SBT–Pt interface. The excess Ta atoms in local regions readily react with O atoms to form TaO_x species that serve as nucleation sites for the crystallization process. This unwanted reaction can, therefore, significantly affect the microstructures and ferroelectric properties of SBT thin films. In this present study, we investigated the effect that the Ta ratio had on the physical and electrical properties of SBT thin films, and herein we suggest possible mechanisms to explain this behavior.

II. EXPERIMENTAL

SBT thin films were prepared using a MOD method. To evaluate the influence of Ta, the molar compositions used in these studies were $SrBi_2Ta_{1.8}O_9$ (Ta-deficient), $SrBi_2Ta_2O_9$ (stoichiometric Ta), and $SrBi_2Ta_{2.2}O_9$ (Ta-rich); for the sake of convenience, these samples are denoted as Ta18, Ta20, and Ta22, respectively. SBT thin films were deposited in multiple layers on top of Pt (150 nm)/TiO_2 (20 nm)/SiO_2/Si substrates. Each layer was spin-coated at 4000 rpm and dried for 10 min at 150 °C, and then the sample was baked at 400 °C for 10 min. After rapid thermal annealing (RTA) at 750 °C under an oxygen atmosphere for 10–60 s, the five-layered SBT exhibited a film thickness of about 200 nm. For electrical measurements, Pt top electrodes were sputtered onto the SBT films through a shadow mask having a diameter of 0.2 mm. The ferroelectric properties of the SBT thin films were measured at room temperature using a RT66A ferroelectric testing system (Radiant Technologies, Albuquerque, NM). The leakage current characteristics of the SBT thin films were studied using a semiconductor parameter analyzer (HP 4156A, Agilent Technologies, Japan). To analyze the physical characteristics, an x-ray diffractometer (XRD; M18XHF-SRA, MAC Science Co., Yokohama, Japan), field-emission scanning electron microscope (FESEM; JEOL JSM-6500F, Tokyo, Japan), and x-ray photoemission spectrometer (XPS; PHI 1600, Physical Electronics USA) were used. The XPS analysis was performed using the Mg K_α line (1253.6 eV). In addition, the C 1*s* peak (284.8 eV) was used to calibrate the measured spectrum. To identify the film compositions of the SBT thin films after crystallization at high temperature, the films were dissolved in an acidic solution and analyzed using inductively coupled plasma (ICP) mass spectrometry. The results indicated the composition ratios were close to those of the precursor solutions. This result implies that the short duration (10–60 s) of the RTA process did not lead to evaporation of any of the elements in the SBT thin film.

III. RESULTS AND DISCUSSIONS

Figure 1(a) displays the polarization–electric field (P–E) curves, measured at ±5 V, of various Pt/SBT/Pt capacitors that had been annealed at 750 °C for 60 s in an oxygen ambient. All the samples exhibited well-defined hysteresis loops, suggesting that each SBT film (with different Ta content) exhibited good ferroelectric properties after high-temperature annealing. Among these

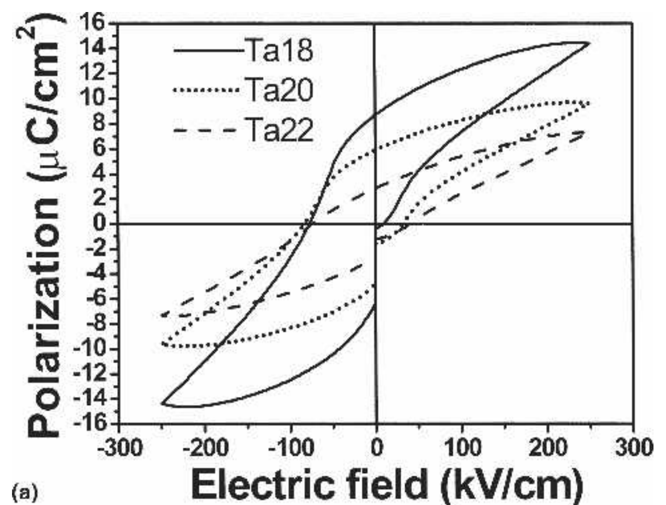

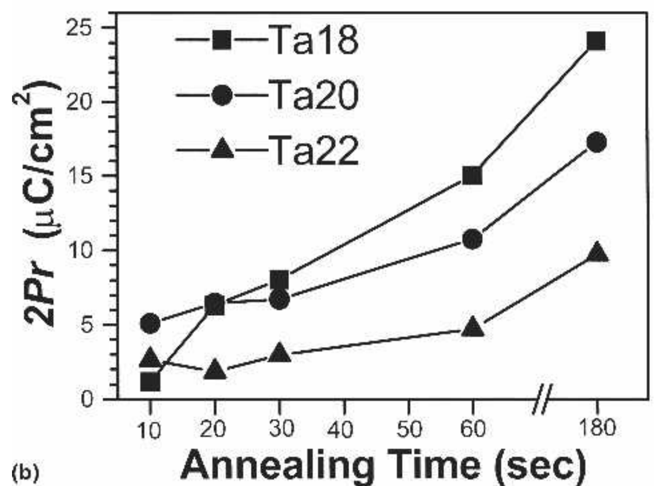

FIG. 1. (a) *P–E* hysteresis loops of SBT thin films deposited on Pt/TiO_2/SiO_2/Si substrates and crystallized at 750 °C for 60 s through RTA in an oxygen ambient. (b) Remanent polarizations of various compositions as a function of the crystallization time.

CAMBRIDGE JOURNALS
http://journals.cambridge.org Downloaded: 26 Apr 2014 IP address: 140.113.38.11

samples, Ta18 seemed to exhibit the best properties. The remanent polarization ($2P_r$) values of Ta18, Ta20, and Ta22 specimens were 15.01, 10.75, and 5.55 $\mu C/cm^2$, respectively, and the coercive fields ($2E_c$) were 87, 115, and 117 kV/cm, respectively. These values confirm that the Ta composition had a dramatic impact on the SBT properties: a reduction of the Ta ratio led to an increase in the value of $2P_r$ of the SBT and a decrease in the value of $2E_c$. Figure 1(b) illustrates the values of the remanent polarization of SBT as a function of the crystallization time (i.e., the duration of RTA at 750 °C). It is evident that, regardless of the Ta ratio, the value of $2P_r$ increased after the annealing time was increased. The tendencies in the values of $2P_r$ as a function of the annealing time were similar for Ta20 and Ta22, but with Ta20 always exhibiting relatively higher values of $2P_r$. Although Ta18 exhibited the best properties in Fig. 1(a), it did not always provide the highest values of $2P_r$ under each set of annealing conditions. After the shortest annealing time (10 s), Ta18 exhibited the worst ferroelectric property. Nevertheless, the rate of increase of $2P_r$ for Ta18 as a function of annealing time was greater than those of the other two specimens (Ta20 and Ta22). As a result, the largest remanent polarizations were observed for Ta18 when the annealing times were longer than 30 s. Although the values of $2P_r$ increased when the annealing time was increased, the leakage current density in SBT rose significantly when the annealing time was increased from 60 to 180 s, possibly because of the larger surface roughness and greater degree of diffusion between SBT and the substrate when crystallization was performed over a longer time. The leakage current might contribute to the higher value of $2P_r$ of SBT; it would be detrimental to the application of SBT to nonvolatile random access memories.

The electrical properties of ferroelectrics generally correspond to their crystallinities and microstructures. To understand the causes of the distinct behavior displayed in Fig. 1 for the SBT samples containing different Ta ratios, we performed physical analyses of these specimens. The x-ray diffraction (XRD) patterns of SBT films after crystallization at 750 °C (Fig. 2) clearly illustrated their polycrystalline structures. In Fig. 2(a), each of the three SBT films, after annealing for 10 s, possessed a mixture of bismuth-layered-structured (BLS) and fluorite phases. Because fluorite is an intermediate structure, its presence implies that the phase transformation in SBT was incomplete. When the annealing time was increased from 10 to 30 s [Figs. 2(a)–2(c)], the peak intensity of the fluorite phase decreased significantly while the BLS peaks became stronger and sharper. Regardless of the annealing duration, Ta18 possessed the lowest amount of fluorite among the three samples; the volume fraction of fluorite in Ta22 was always greater than that in Ta20. By further extending the annealing time, the amount of BLS continued to increase, with the accompanying decrease of the signal for fluorite. Figure 3(a) presents the tendency of the integrated intensity ratios of the fluorite (111) to BLS (115) reflections $\{I_{F(111)}/[I_{B(115)} + I_{F(111)}]\}$ as a function of annealing time; here, $I_{F(111)}$ is the integrated intensity of the (111) reflection of the fluorite phase. After annealing for 60 s, Ta18 possessed a nearly pure BLS phase, but slight and considerable amounts of fluorite phases were still detectable for Ta20 and Ta22, respectively. Because the fluorite phase is nonferroelectric, the existence of fluorite degrades the ferroelectric properties of SBT. Furthermore, it is worth noting that not only the crystallinities changed with respect to the Ta ratio but so did the textures of the SBT samples. Figure 3(b) indicates that the intensity ratios of the (200) peaks ($I_{(200)}/[I_{(115)} + I_{(200)}]$) of the BLS phases varied with respect to the annealing time. [In Fig. 3, we excluded the BLS (220) orientation from the calculations because the overlap between the Pt (200) and BLS (220) peaks would possibly obstruct the results.] Because the ferroelectric properties are much better along the *a-b* axes of preferentially oriented SBT, this intensity ratio should indicate the degree of preferential orientation along the *a* and *b* axes as well as the ferroelectric properties. As indicated in Fig. 3(b), Ta18 exhibited the highest BLS (200) intensity ratios among all the specimens, regardless of the annealing time. In addition, it seems that the texture of the SBT sample depended strongly on its Ta content and slightly on the annealing duration. To summarize the XRD analyses, Ta18 displayed superior preferential orientation and a higher extent of crystallization. Based on these results, Ta18 should exhibit the greatest ferroelectric properties among all of these specimens under all of the annealing conditions. This hypothesis holds true for the samples that had been annealed for longer than 30 s, but it was clearly not the case for shorter crystallization times. Thus, there must be other factors that affect the ferroelectric properties of the SBT samples, such as the microstructures of the SBT films.

We used the FESEM to examine the surface morphologies of the SBT thin films (Fig. 4). The SBT films that had been crystallized for 10 s were composed of mostly nano-sized grains [Figs. 4(a)–4(c)], although we observed some elliptical grains with sizes greater than 70 nm for Ta20 [Fig. 4(b)]. These large grains are the typical BLS grain structure.[18,19] We believe that the appearance of these large grains is the reason for the relatively high value of $2P_r$ in Ta20. Although the Ta18 sample possessed the greatest volume fraction of the ferroelectric BLS phase, its BLS grains were not sufficiently large. It has been reported that the electrical properties of ferroelectrics depend strongly on their grain sizes.[20] When the grains are smaller than a critical size, the ferroelectrics exhibit only weak ferroelectric behavior. In Ta18, each grain had a size smaller than 40 nm

CAMBRIDGE JOURNALS http://journals.cambridge.org Downloaded: 26 Apr 2014 IP address: 140.113.38.11

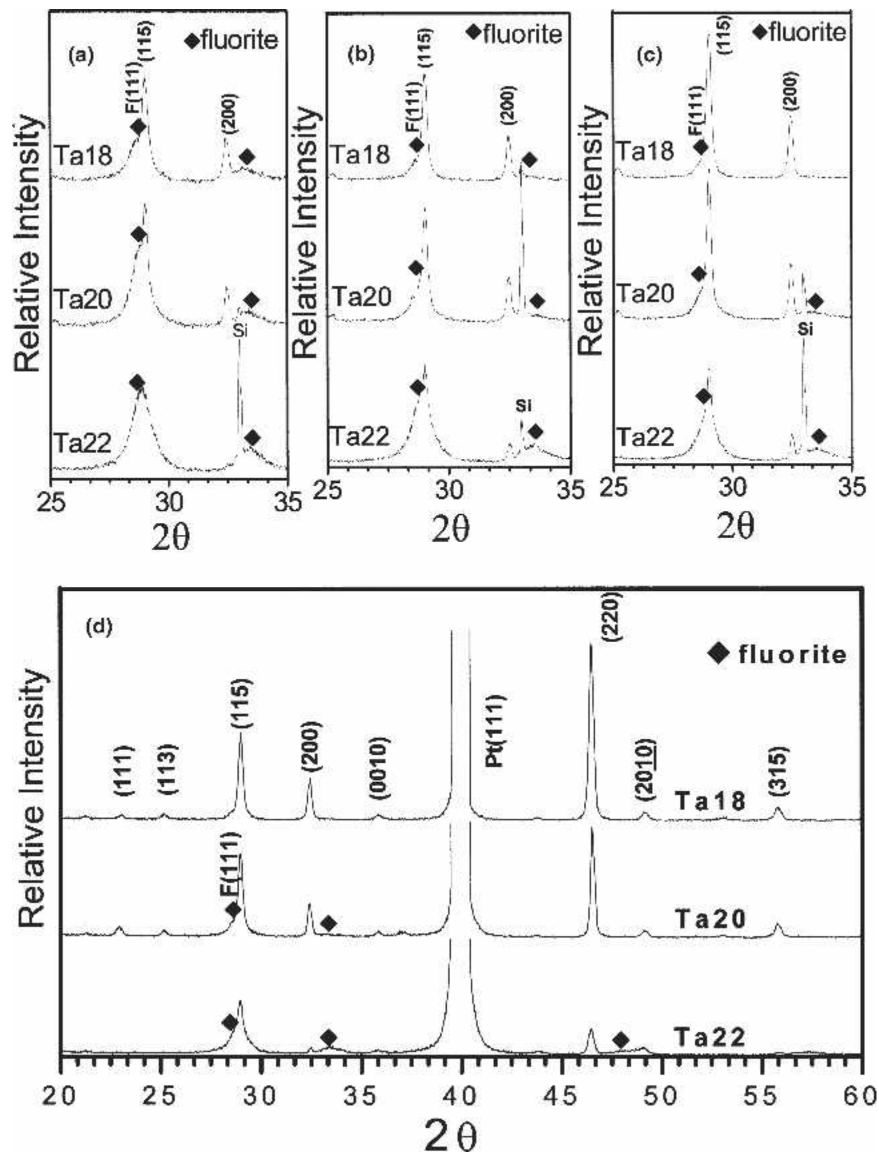

FIG. 2. XRD patterns of the SBT thin films that had been crystallized at 750 °C for (a) 10 s, (b) 20 s, (c) 30 s, and (d) 60 s. The Si peak originated from the silicon substrate.

[Fig. 4(a)]. For this reason, we speculate that Ta18 will display poor ferroelectric properties if the annealing time is insufficient to produce large grains. In contrast, an abundance of large grains was produced in Ta18 when the annealing time was greater than 30 s [Fig. 4(d)]. Under these conditions, the volume fraction of large grains (~90 nm) in Ta18 exceeded that in Ta20 [Fig. 4(e)]. When we extended the annealing time further to 60 s, uniformly large grain structures developed in Ta18 [Figs. 5(a) and 5(b)], whereas Ta20 [Figs. 5(c) and 5(d)] retained a considerable volume of nano-sized grains. Moreover, the growth of such large grains was considerably slower in Ta22; only a few large grains emerged in the nano-grain matrix even after the sample was subjected to a relatively long annealing time of 60 s [Figs. 5(e) and 5(f)]. The changes in the microstructures of the SBT samples reflect the fact that the growth rates of the BLS phase depend strongly on the Ta ratio in SBT; indeed, the growth rate increased upon decreasing the Ta content from Ta-rich (Ta22) to Ta-deficient (Ta18) SBT. To summarize the physical analyses from the XRD and SEM results, we found that the microstructures, textures, and phase constitutions were all closely related to the Ta ratios in the SBT samples. The fast transformation of fluorite to the BLS phase and the rapid BLS growth rate were the major factors contributing to the ultimately uniform and large grain structures in Ta18. This result implies that the nucleation and growth processes of the BLS grains were more pronounced in Ta18 than they were in either Ta20 or Ta22.

Because the ionic radii of Sr (1.16 Å) and Bi (1.03 Å) are much greater than that of Ta (0.64 Å),[11,20] a deficiency in

CAMBRIDGE JOURNALS
http://journals.cambridge.org Downloaded: 26 Apr 2014 IP address: 140.113.38.11

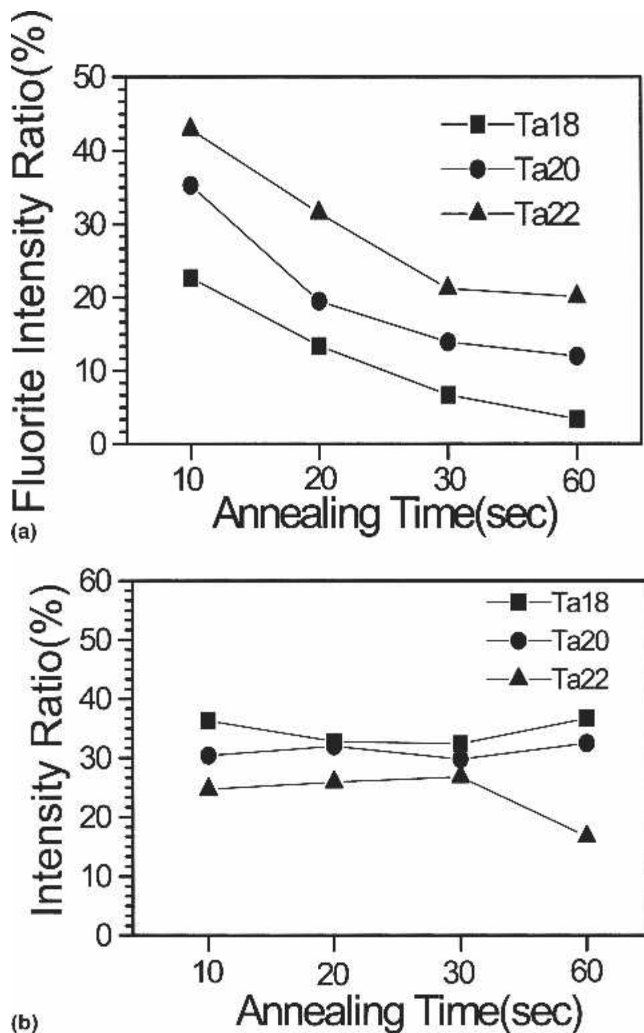

FIG. 3. (a) Intensity ratios $\{I_{F(111)}/[I_{B(115)} + I_{F(111)}]\}$ of the fluorite phase and (b) texturing ratios $\{I_{(200)}/[I_{(115)} + I_{(200)}]\}$ of SBT films containing different Ta contents as a function of annealing time.

Ta cannot be compensated well by an excess of Sr or Bi. Based on defect chemistry, the deficiency of Ta atoms in the $SrBi_2Ta_{1.8}O_9$ film would be accompanied by the occurrence of cation vacancies and holes:

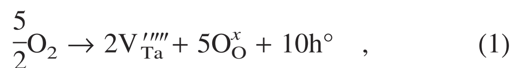

$$\frac{5}{2}O_2 \rightarrow 2V_{Ta}^{'''''} + 5O_O^x + 10h^\circ \quad , \qquad (1)$$

where $V_{Ta}^{'''''}$ indicates a negatively charged vacancy (relative to a perfect lattice) on the Ta site, O_O^x denotes an oxygen atom on the oxygen site, and h° represents a hole. The existence of cation vacancies and holes can be proved by the variations of conductivity in SBT. The measured conductivity of the Ta18 sample annealed for 60 s was greater than those of the other two samples (Table I). This result may be due to the induction of *p*-type charge carriers (holes) in Ta18.[21,22] Whereas a higher conductivity might lead to apparently higher polarization, the leakage current density of each of these three samples (Ta18, Ta20, and Ta22) was lower than 3.7×10^{-7} A/cm^2 under an applied electric field of 130 kV/cm. The current densities of these SBT samples are comparable to those (10^{-6}–10^{-7} A/cm^{-2}) reported previously.[23–25] If our hypothesis is correct, a large number of Ta^{+5} vacancies would be generated within the Ta-deficient SBT. Because the Ta–O bonding strength is greater than those of Sr–O and Bi–O bonds, the diffusion coefficient of Ta ($<10^{-17}$ cm^2/s) in SBT is much lower than those of the Sr (10^{-15} cm^2/s) and Bi (10^{-14} cm^2/s) atoms, as measured from the SBT species in a SiO_2 layer at 800 °C.[26] We believe that the diffusion behavior of SBT in our present study is controlled by the constituted Ta ions and is accelerated significantly by the generation of Ta^{+5} vacancies. Therefore, both the nucleation and growth of the BLS grains in Ta18 would be promoted by the deficiency of Ta ions in the material. The existence of Ta^{+5} vacancies also affects the polarization-switching properties of ferroelectrics.[27] Because the defects can act as nuclei,[28] the energy barrier for the nucleation of ferroelectric domains was significantly lowered by the existence of Ta^{+5} vacancies, leading to a lower value of E_c. This result corresponds well with the low value of E_c of Ta18 observed in our P–E analysis (Fig. 1). On the other hand, a Ta deficiency can also be regarded as an excess of Sr and Bi in SBT. Although an excess of Bi in Sr-deficient SBT has been proven to improve the material's properties, few studies describe the variations of the properties of SBT when Bi and Sr are both present in excess.[13,15] The only example of which we are aware is that of a study of $Sr_{1.2}Bi_{2.3}Ta_2O_9$ films by Chen et al.; their experimental results—poor ferroelectric properties—are in contrast to ours.[15] Although similar to Ta18, the Ta/Sr and Ta/Bi ratios in Chen's samples were lower than stoichiometric; the starting compositions of the SBT samples were quite different in the two sets of experiments. Further examinations are necessary if we are to understand the roles of Sr, Bi, and Ta and their ratios in SBT samples.

It was possible that the SBT films possessed the following three types of defects: O vacancies, Ta vacancies, and Bi vacancies. The ferroelectric Aurivillius phases of $SrBi_2Ta_2O_9$ consist of layers of perovskite-like blocks $[(SrTa_2O_7)^{2-}]$ sandwiched between two consecutive $(Bi_2O_2)^{2+}$ layers. The oxygen ions in the $SrTa_2O_7$ perovskite layers are much more stable than those within the Bi_2O_2 layers. Therefore, for SBT thin films, oxygen atom vacancies occur preferentially in the Bi_2O_2 layers.[29] We speculated that the deficiency of Ta in Ta18 films contributed to Ta vacancies, and the redundant oxygen atoms would stabilize (or compensate) the oxygen ions (vacancies) in the $SrTa_2O_7$ octahedra or Bi_2O_2 layers. In contrast, the excess of Ta atoms would contribute to the oxygen atom vacancies in $SrTa_2O_7$ octahedra. This extra amount of Ta in Ta22 would cause oxygen ions to become unstable, either at the $SrTa_2O_7$ octahedra or Bi_2O_2

CAMBRIDGE JOURNALS
http://journals.cambridge.org Downloaded: 26 Apr 2014 IP address: 140.113.38.11

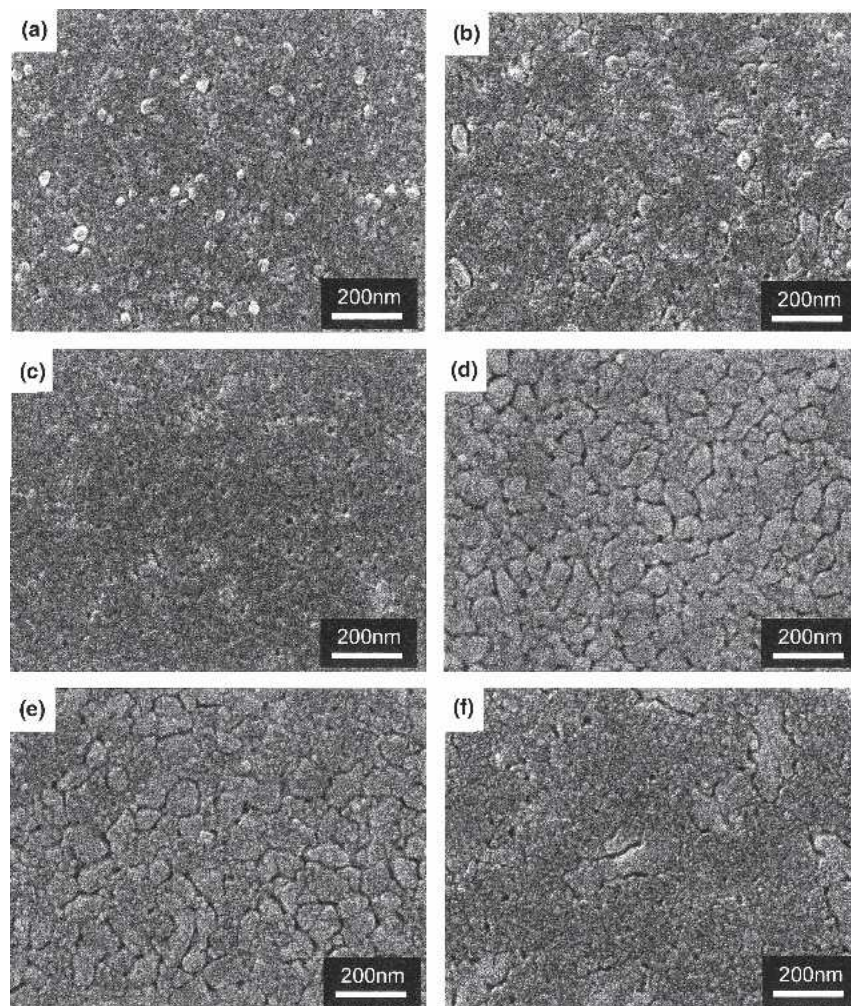

FIG. 4. FESEM planar images of SBT thin films: (a) Ta18, (b) Ta20, and (c) Ta22 annealed at 750 °C for 10 s,; (d) Ta18, (e) Ta20, and (f) Ta22 annealed at 750 °C for 30 s.

layers. As discussed above, a deficiency of Ta could introduce extra Ta vacancies into the SBT film. The incorporation of such vacancies would also affect the chemical bonding conditions of SBT. XPS is a sensitive technique that can distinguish between local electronic structures when the chemical nature of a specimen is probed. We conducted XPS analyses of the SBT film surfaces to study the changes in the chemical states of Ta at various Ta contents. Figure 6 displays the XPS spectra of the Ta 4*f* core levels for the samples before [Figs. 6(a)–6(c)] and after [Figs. 6(d)–6(f)] argon-ion sputtering for 60 s. To identify the contributions of the different oxidation states, it was necessary to perform a deconvolution (peak fitting) of the measured spectra with respect to the different chemical shifts. The ratio of the intensities of the doublet components (Ta 4*f* core levels) was determined using the respective ratio of the occupation number of the subshell states [i.e., (Ta $4f_{7/2}$)/(Ta $4f_{5/2}$) = 4/3]. After correction for the spectral background using Shirley's method,[30] we decomposed the spectra into the Gaussian–Lorentzian profiles associated with metallic Ta and Ta in Ta_2O_5 and suboxides, respectively. Table II lists the fitting peak positions for metallic Ta and its associated oxides; Table III summarizes the entire measured chemical bonding states of Ta atoms in the different SBT samples. The sequences illustrate the relative amounts of the various chemical states in the specimens (high to low). In Fig. 6, the solid line represents the real spectrum, while the curve of circular symbols represents the fitted one. The Ta 4*f* spectrum obtained from the Ta18 sample [Fig. 6(a)] was deconvoluted into two $4f_{7/2}$ peaks at 26.6 and 27.4 eV. We attribute the binding energy of 26.6 eV to Ta_2O_5, the highest oxidation state of tantalum. The other peak (at 27.4 eV) might be related to the TaO_x complex. The binding energy in TaO_x is 0.8 eV higher than that in Ta_2O_5, implying that more electronegative species are involved in the bonds.[31] This species was possibly a negatively charged Ta vacancy or oxygen ion. Figures 6(b) and 6(c) depict the deconvoluted XPS peaks from

CAMBRIDGE JOURNALS
http://journals.cambridge.org Downloaded: 26 Apr 2014 IP address: 140.113.38.11

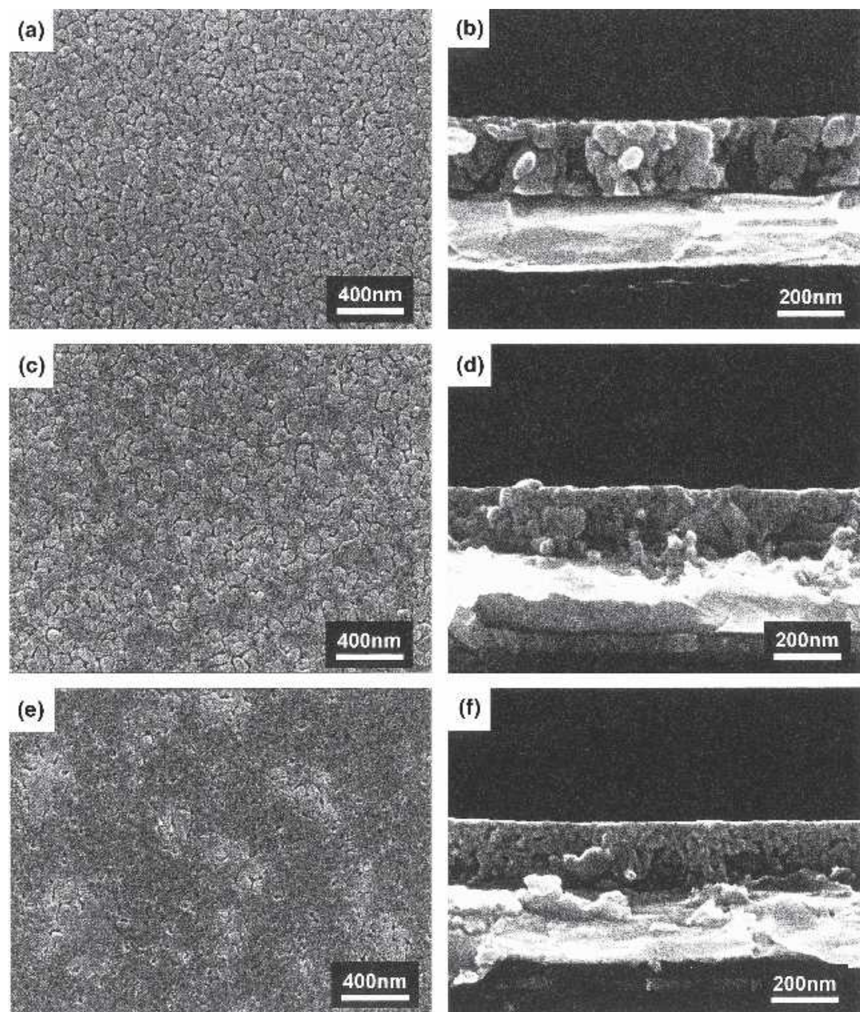

FIG. 5. FESEM planar and cross-sectional images of SBT thin films after crystallization at 750 °C for 60 s: (a,b) Ta18, (c,d) Ta20, and (e,f) Ta22.

TABLE I. AC conductivities (measured at 10 Hz and room temperature) of SBT films incorporating different Ta contents.

	Ta18	Ta20	Ta22
Conductivity (Ω^{-1} cm^{-1})	9.55×10^{-10}	9.25×10^{-12}	1.4852×10^{-12}

the Ta20 and Ta22 samples, respectively. The $4f_{7/2}$ peaks at 25.9, 26.6, and 27.4 eV indicate the presence of TaO_2, Ta_2O_5, and TaO_x, respectively; i.e., a new Ta oxidation state (TaO_2) occurred in Ta20 and Ta22 that was absent in Ta18. Because the well-bonded Ta atoms in SBT exhibit an oxidation state of Ta_2O_5, the presence of TaO_2 implies that some of the Ta atoms in the perovskite layers of SBT were not fully bonded and, possibly, were associated with the oxygen vacancies. In addition, the relative amount of TaO_2 in Ta22 was greater than that in Ta20, indicating that the extra Ta in SBT caused an increase in the number of embedded oxygen vacancies. Figures 6(d)–6(f) present the XPS spectra of the Ta 4*f* core levels for sputtered Ta18, Ta20, and Ta22, respectively. We performed this sputtering with argon ions to remove any residual contamination on the films' surfaces. In addition, any changes in the nature of the chemical states after ion bombardment could be useful to understanding the stability of the tantalum oxides. After sputtering, we observed no new chemical states for Ta18 [Fig. 6(d)] or Ta20 [Fig. 6(e)], but the relative intensities of the Ta states had changed slightly. The intensity ratio of TaO_x decreased, accompanied by increases in the ratios of TaO_2 and Ta_2O_5; this result suggests that the TaO_x bond is relatively unstable. In contrast, we observed significant changes in the XPS spectrum in Ta22 after sputtering [Fig. 6(f)]; new chemical states appeared at lower energy—22.1 and 23.8 eV—which corresponded to metal-like Ta ($4f_{7/2}$) and TaO ($4f_{7/2}$) states, respectively.[32] Although we could not confirm definitively which of the bonds contributed to the formation of the metal-like Ta and TaO during ion bombardment, this result does clearly reflect the fact that the Ta–O bonds in Ta22 were less stable than those in Ta18 and Ta20. The weakness of the Ta–O bonds in Ta22 might have arisen from the

CAMBRIDGE JOURNALS http://journals.cambridge.org Downloaded: 26 Apr 2014 IP address: 140.113.38.11

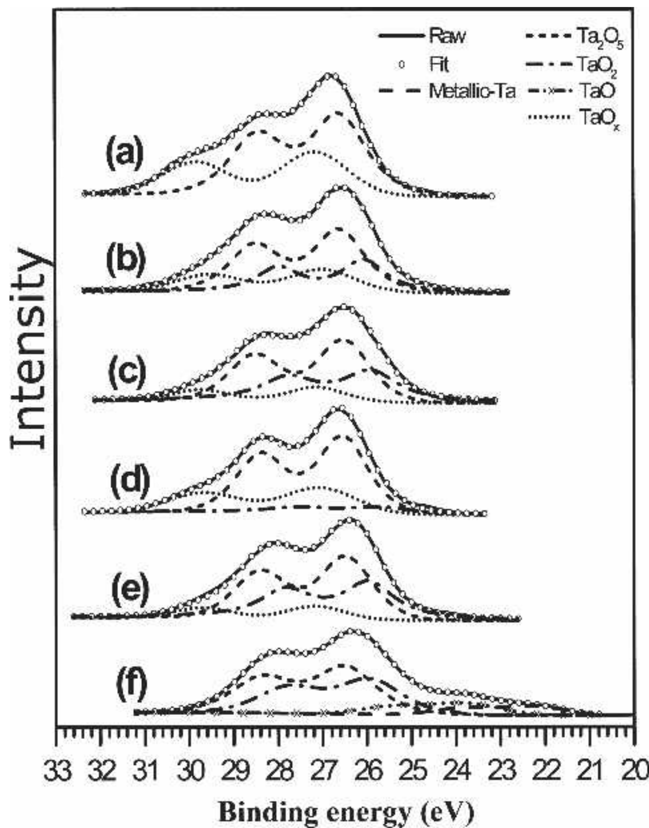

FIG. 6. Deconvoluted Ta (4*f*) XPS spectra obtained from the surfaces of SBT samples before [(a) Ta18, (b) Ta20, (c) Ta22] and after [(d) Ta18, (e) Ta20, and (f) Ta22] argon ion sputtering. Each specimen was crystallized at 750 °C for 60 s. Solid lines: experimental data; dashed lines: deconvoluted components; circular symbols: sums of deconvoluted components.

excess of Ta atoms, which were difficult to fully oxidize, leading to the presence of oxygen vacancies and the observed poor ferroelectric properties. In our previous paper, we reported that the use of a Ta buffer layer enriched the Ta content near the SBT/Pt interface and improved the SBT properties.[17] Because the Ta buffer layer was ultrathin (<0.3 nm), the bulk composition of the SBT film was barely influenced by the presence of the buffer layer. Therefore, it is reasonable that we have obtained distinct SBT properties for the Ta22 specimen and for the SBT sample possessing a Ta buffer layer. When the buffer layers became thicker (~1 nm), the abundance of Ta ions resulted in a significant change in the SBT composition near the SBT–Pt interface, which degraded the properties of the SBT sample. This finding suggested that an SBT sample possessing an excessively thick Ta film layer would exhibit poor properties. This situation is similar to the properties displayed by the Ta22 specimen in the present study.

We tested the fatigue endurance of the materials by applying 1 MHz bipolar pulses at 5 V. Figure 7 displays the normalized polarizations (P_{NV}, $P^* - \hat{P}$) of the SBT

TABLE II. Photospectroscopic peak positions for Ta and its oxides. Observed positions are those of Ta22; they exhibited a systematic shift of ~0.2 eV from the expected values as a result of instrumental offset.

Peak	Observed position (eV)	Expected position (eV)
Ta $4f_{5/2}$	23.9	23.8[a]
Ta $4f_{7/2}$	22.1	21.9[a]
$TaO4f_{5/2}$	25.6	25.8 ± 0.4[b]
$TaO4f_{7/2}$	23.8	24.0 ± 0.4[b]
$TaO_24f_{5/2}$	27.7	27.8 ± 0.4[b]
$TaO_24f_{7/2}$	25.9	26.0 ± 0.4[b]
$Ta_2O_54f_{5/2}$	28.4	28.6 ± 0.2[b]
$Ta_2O_54f_{7/2}$	26.6	26.8 ± 0.2[b]
$TaO_x4f_{5/2}$	29.9	
$TaO_x4f_{7/2}$	27.4	27.8 ± 0.2[c]

[a]*Handbook of X-ray Photoelectron Spectroscopy, Physical Electronics* (Perkin-Elmer Corporation, Eden Prairie, MN, 1992).
[b]Ref. 32.
[c]Ref. 31.
C 1*s* = 284.8 eV.

TABLE III. Relative amounts (high to low) of Ta oxidation states in different SBT films, as measured from XPS spectra.

	As-deposited	Sputtered
Ta18	Ta_2O_5, TaO_x	Ta_2O_5, TaO_x, TaO_2
Ta20	Ta_2O_5, TaO_x, TaO_2	Ta_2O_5, TaO_2, TaO_x
Ta22	Ta_2O_5, TaO_2, TaO_x	Ta_2O_5, TaO_2, TaO, Ta

capacitors (which had been prepared at 750 °C for 60 s) as a function of the number of polarization switching cycles. All of the SBT films exhibited nearly fatigue-free characteristics after 10^{10} cycles. It has been reported that the fatigue behavior correlates with the nature of the defect traps at the domain boundaries.[33,34] We expected that the Ta-deficient (Ta18) and Ta-rich (Ta22) SBT

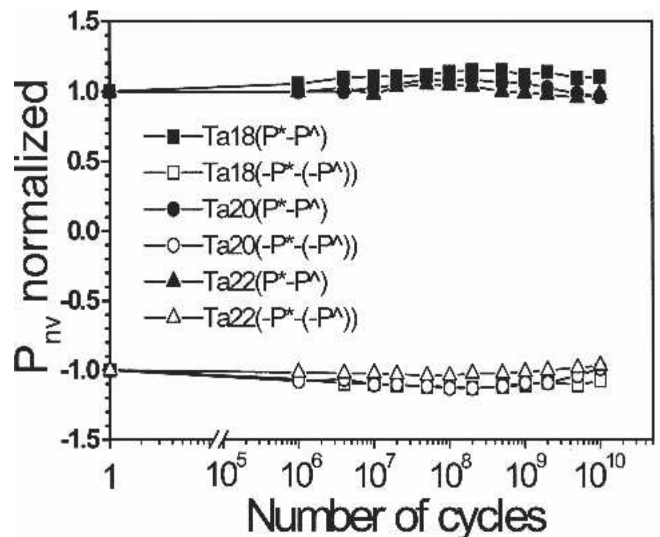

FIG. 7. Fatigue characteristics of Ta18, Ta20, and Ta22 samples annealed at 750 °C for 60 s. This test was performed using bipolar pulses of 1 MHz at an amplitude of 250 kV/cm.

CAMBRIDGE JOURNALS
http://journals.cambridge.org Downloaded: 26 Apr 2014 IP address: 140.113.38.11

films would each exhibit an abundance of defect states (such as Ta or O vacancies) and significant fatigue behavior. However, our present analyses indicated only slight degrees of fatigue in Ta18 and Ta22. Robertson et al. studied the electronic structures of SBT materials and reported that the electrons are shallowly trapped at the Ta^{5+} or Bi^{3+} ions and are readily detrapped.[35] Therefore, the fatigue characteristics in SBT samples degraded slightly as a result of the appearance of these defects (Ta or O vacancies).

IV. CONCLUSIONS

We have investigated the effect that the Ta content has on the electrical and physical properties of SBT materials. A Ta-deficient SBT sample (Ta18) exhibited superior crystallinity, texture, and microstructure relative to those properties of the stoichiometric (Ta20) or Ta-rich (Ta22) SBT species. After annealing at 750 °C for 60 s, Ta18 exhibited a uniform BLS structure, whereas we detected a considerable amount of a second-phase (fluorite) in the Ta-rich SBT. Because Ta18 also displayed a relatively high (200) preferential orientation, we observed better ferroelectric properties in this Ta-deficient SBT material. We attribute the improved properties of Ta-deficient SBT to the presence of Ta vacancies, the existence of which was supported by conductivity measurements and XPS analyses. The SBT thin films possessing a 10% Ta deficiency exhibited negligible fatigue degradation (<4%) at up to 10^{10} switching cycles, which makes such materials competitive for use in memory applications.

ACKNOWLEDGMENTS

We are grateful to the staff of the National Nano Device Laboratories, Hsinchu, Taiwan, for providing technical support. This study was supported by the National Science Council, Republic of China, through Contract No. 93-2215-E492-010.

REFERENCES

1. C.A. Paz de Araujo, J.D. Cuchiaro, L.D. McMillan, M.C. Scott, and J.F. Scott: Fatigue-free ferroelectric capacitors with platinum electrodes. *Nature* **374,** 627 (1995).
2. A.D. Li, D. Wu, H.Q. Ling, T. Yu, M. Wang, X.B. Yin, Z.G. Liu, and N.B. Ming: Effects of processing on the characteristics of $SrBi_2Ta_2O_9$ films prepared by metalorganic decomposition. *J. Appl. Phys.* **88,** 1035 (2000).
3. R. Dat, J.K. Lee, O. Auciello, and A.I. Kingon: Pulsed laser ablation synthesis and characterization of layered $Pt/SrBi_2Ta_2O_9/Pt$ ferroelectric capacitors with practically no polarization fatigue. *Appl. Phys. Lett.* **67,** 572 (1995).
4. N.J. Seony, C.H. Yang, W.C. Shin, and S.G. Yoon: Oxide interfacial phases and the electrical properties of $SrBi_2Ta_2O_9$ thin films prepared by plasma-enhanced metalorganic chemical vapor deposition. *Appl. Phys. Lett.* **72,** 1374 (1998).
5. R.W. Vest: Metallo-organic decomposition (MOD) processing of ferroelectric and electrooptic films: A review. *Ferroelectrics* **102,** 53 (1990).
6. K. Franke, G. Matin, M. Weihnacht, and A.V. Sotnikov: $SrBi_2Ta_2O_9$ has only two polar axes—A problem for high density ferroelectric memory devices. *Solid State Commun.* **119,** 117 (2001).
7. T.A. Derouin, C.D.E. Lakeman, X.H. Wu, J.S. Speak, and F.F. Lange: Effect of lattice mismatch on the epitaxy of sol-gel $LiNbO_3$ thin films. *J. Mater. Res.* **12,** 1391 (1997).
8. Y.H. Xu, C.H. Cheng, Y.D. Lou, and J.D. Mackenzie: Epitaxial ferroelectric thin films prepared by the sol-gel technique. *Ferroelectrics* **195,** 283 (1998).
9. R. Ramesh, J. Lee, T. Sands, V.G. Keramidas, and O. Auciello: Oriented ferroelectric La–Sr–Co–O/Pb–La–Zr–Ti–O/La–Sr–Co–O heterostructures on [001] Pt/SiO_2 Si substrates using a bismuth titanate template layer. *Appl. Phys. Lett.* **64,** 2511 (1994).
10. T. Hayashi, H. Takahashi, and T. Hara: Chemical processing and dielectric properties of ferroelectric $SrBi_2Ta_2O_9$ thin films. *Jpn. J. Appl. Phys.* **35,** 4952 (1996).
11. T. Atsuki, N. Soyama, T. Yonezawa, and K. Ogi: Preparation of Bi-based ferroelectric thin films by sol-gel method. *Jpn. J. Appl. Phys., Part 1* **34,** 5096 (1995).
12. K. Miura and M. Tanaka: The effect of Bi ions substituting at the Sr site in $SrBi_2Ta_2O_9$. *Jpn. J. Appl. Phys., Part 1* **37,** 2554 (1998).
13. T. Noguchi, T. Hase, and Y. Miyasaka: Analysis of the dependence of ferroelectric properties of strontium bismuth tantalate (SBT) thin films on the composition and process temperature. *Jpn. J. Appl. Phys., Part 1* **35,** 4900 (1996).
14. Y. Shimakawa, Y. Kubo, Y. Nakagowa, T. Kamiyama, H. Asano, and F. Izumi: Crystal structures and ferroelectric properties of $SrBi_2Ta_2O_9$ and $Sr_{0.8}Bi_{2.2}Ta_2O_9$. *Appl. Phys. Lett.* **74,** 1904 (1999).
15. S-Y. Chen and V-C. Lee: Effect of lead additive on the ferroelectric properties and microstructure of $Sr_xPb_yBi_{2z}Ta_2O_9$ thin films. *J. Appl. Phys.* **87,** 8024 (2000).
16. T. Hase, T. Noguchi, K. Amanuma, and Y. Miyasaka: Sr content dependence of ferroelectric properties in $SrBi_2Ta_2O_9$ thin films. *Integr. Ferroelectr.* **15,** 127 (1997).
17. C.C. Leu, C.H. Chien, F.Y. Hsu, H-T. Lin, and C.T. Hu: Influence of ultrathin tantalum buffer layers on microstructure and ferroelectric properties of $SrBi_2Ta_2O_9$ thin films. *J. Electrochem. Soc.* **151,** F167 (2004).
18. S.B. Ren, C.J. Lu, H.M. Shen, and Y.N. Wang: Size-related ferroelectric-domain-structure transition in a polycrystalline $PbTiO_3$ thin film. *Phys. Rev. B.* **54,** R14337 (1996).
19. S.B. Ren, C.J. Lu, H.M. Shen, and Y.N. Wang: In situ study of the evolution of domain structure in free-standing polycrystalline $PbTiO_3$ thin films under external stress. *Phys. Rev. B.* **55,** 3485 (1997).
20. W.C. Kwak and Y-M. Sung: Crystallization kinetics of sol-gel-derived $(1-x)SrBi_2Ta_2O_9$–xBi_3TiTaO_9 ferroelectric thin films. *J. Mater. Res.* **17,** 1463 (2002).
21. S. Bhattacharyya, A. Laha, and S.B. Krupanidhi: Impact of Sr content on dielectric and electrical properties of pulsed laser ablated $SrBi_2Ta_2O_9$ thin films. *J. Appl. Phys.* **92,** 1056 (2002).
22. C.M. Palanduz and D.M. Smyth: The effect of cation place exchange on the electrical conductivity of $SrBi_2M_2O_9$ (M = Ta, Nb). *J. Eur. Ceram. Soc.* **19,** 731 (1999).
23. W.C. Shin and S.G. Yoon: Improvement in ferroelectric properties of $SrBi_2Ta_2O_9$ thin films with Bi_2O_3 buffer layers by liquid-delivery metalorganic chemical-vapor deposition. *Appl. Phys. Lett.* **79,** 1519 (2001).

CAMBRIDGE JOURNALS http://journals.cambridge.org Downloaded: 26 Apr 2014 IP address: 140.113.38.11

24. S.Y. Chen, B.C. Lan, and C.S. Taso: Film structure and ferroelectric properties of vanadium-doped $Sr_{0.8}Bi_{2.3}Ta_2O_9$ thin films. *J. Appl. Phys.* **91,** 10032 (2002).
25. S.H. Kim, D.J. Kim, J.P. Maria, A.I. Kingon, S.K. Streiffer, J. Im, O. Auciello, and A.R. Krauss: Influence of Pt heterostructure bottom electrodes on $SrBi_2Ta_2O_9$ thin film properties. *Appl. Phys. Lett.* **76,** 496 (2000).
26. R. Bungener, W. Pamler, and U. Gosele: Diffusion of Sr, Bi, and Ta in amorphous SiO_2. *Mater. Sci. Semicond. Process.* **6,** 43 (2003).
27. Q. Tan, J. Li, and D. Viehland: Role of lower valent substituent-oxygen vacancy complexes in polarization pinning in potassium-modified lead zirconate titanate. *Appl. Phys. Lett.* **75,** 418 (1999).
28. D. Viehland and Y.H. Chen: Random-field model for ferroelectric domain dynamics and polarization reversal. *J. Appl. Phys.* **88,** 6696 (2000).
29. B.H. Park, S.J. Hyun, S.D. Bu, T.W. Noh, J. Lee, H-D. Kim, T.H. Kim, and W. Jo: Differences in nature of defects between $SrBi_2Ta_2O_9$ and $Bi_4Ti_3O_{12}$. *Appl. Phys. Lett.* **74,** 1907 (1999).
30. D.A. Shirley: High-resolution x-ray photoemission spectrum of the valence bands of gold. *Phys. Rev. B* **5,** 4709 (1972).
31. J.H. Thomas III and L.H. Hammer: A photoelectron spectroscopy study of carbon tetrafluoride/hydrogen reactive ion etching residue on tantalum disilicide. *J. Electrochem. Soc.* **136,** 2004 (1989).
32. S. Hofman and J.M. Sanz: Quantitative XPS analysis of the surface layer of anodic oxides obtained during depth profiling by sputtering with 3 keV Ar^+ ions. *J. Trace Microprobe Technol.* **1,** 213 (1982).
33. G.L. Yuan, J-M. Liu, Y.P. Wang, D. Wu, S.T. Zhang, Q.Y. Shao, and Z.G. Liu: Fatigue study of metalorganic-decomposition-derived $SrBi_2Ta_2O_9$ thin films: The effect of partial switching. *Appl. Phys. Lett.* **76,** 2208 (2000).
34. D. Wu, A. Li, H. Ling, T. Yu, Z. Liu, and N. Ming: Temperature-dependent fatigue behaviors of ferroelectric ABO_3-type and layered perovskite oxide thin films. *Appl. Phys. Lett.* **84,** 3352 (2004).
35. J. Robertson, C.W. Chen, W.L. Warren, and C.D. Gutleben: Electronic structure of the ferroelectric layered perovskite $SrBi_2Ta_2O_9$. *Appl. Phys. Lett.* **69,** 1704 (1996).

CAMBRIDGE JOURNALS
http://journals.cambridge.org Downloaded: 26 Apr 2014 IP address: 140.113.38.11